AD-A060 979 ENVIRONMENTAL RESEARCH INST OF MICHIGAN ANN ARBOR AP--ETC F/G 17/8
BASIC REMOTE SENSING INVESTIGATION FOR BEACH RECONNAISSANCE - B--ETC(U)
JUL 78 D R LYZENGA, F J THOMSON N00014-74-C-0273
UNCLASSIFIED ERIM-108900-11-F NL

| OF |
AD
A060 979

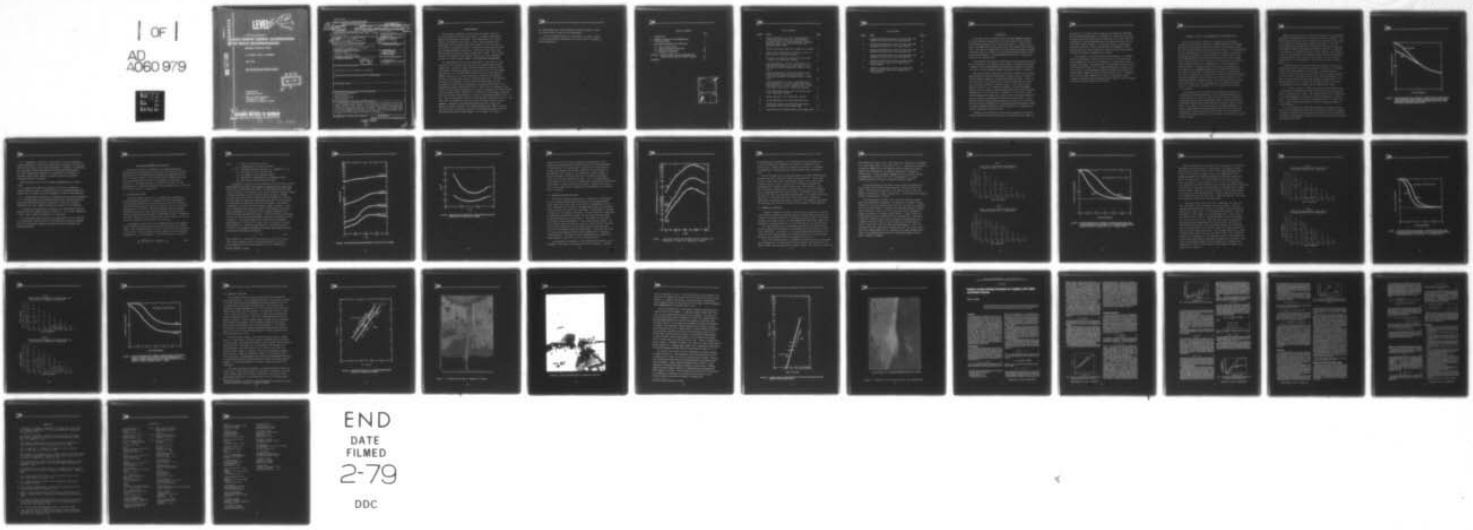

END
DATE
FILMED
2-79
DDC

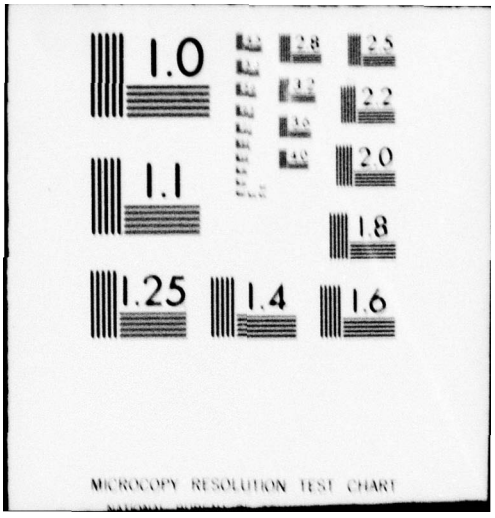
1.0
1.1
1.25
1.4
1.6
2.0
1.8
2.2
2.5
MICROCOPY RESOLUTION TEST CHART

108900-11-F

LEVEL III (12)

A044836

Final Technical Report

BASIC REMOTE SENSING INVESTIGATION FOR BEACH RECONNAISSANCE-

Bottom Features Task

D. LYZENGA AND F. THOMSON

JULY 1978

Prepared for:
Geography Branch

Office of Naval Research
Arlington, VA 22217
Contract No. N0014-74-C-0273

ENVIRONMENTAL
RESEARCH INSTITUTE OF MICHIGAN
FORMERLY WILLOW RUN LABORATORIES, THE UNIVERSITY OF MICHIGAN
BOX 8618 • ANN ARBOR • MICHIGAN 48107

UNCLASSIFIED

SECURITY CLASSIFICATION OF THIS PAGE (When Data Entered)

REPORT DOCUMENTATION PAGE

READ INSTRUCTIONS BEFORE COMPLETING FORM

1. REPORT NUMBER: 108900-11-F (ERIM)	2. GOVT ACCESSION NO. (9) Final rept.	3. RECIPIENT'S CATALOG NUMBER: 1 Jan 74-28 Feb 78
4. TITLE (and Subtitle): Final Technical Report, BASIC REMOTE SENSING INVESTIGATION FOR BEACH RECONNAISSANCE - Bottom Features Task.		5. TYPE OF REPORT & PERIOD COVERED: Final Report 1-1-74 to 2-28-78
		6. PERFORMING ORG. REPORT NUMBER: 108900-11-F ✓
7. AUTHOR(s): (10) David R. Lyzenga and Fred J. Thomson		8. CONTRACT OR GRANT NUMBER(s): (15) N0014-74-C-0273
9. PERFORMING ORGANIZATION NAME AND ADDRESS: Environmental Research Institute of Michigan, Applications Division, P.O. Box 8618, Ann Arbor, Michigan 48107		10. PROGRAM ELEMENT, PROJECT, TASK AREA & WORK UNIT NUMBERS
11. CONTROLLING OFFICE NAME AND ADDRESS: Geography Branch, Office of Naval Research, Arlington, Virginia 22217		12. REPORT DATE: (11) JUL 1978
		13. NUMBER OF PAGES
14. MONITORING AGENCY NAME AND ADDRESS (if different from Controlling Office)		15. SECURITY CLASS. (of this report): Unclassified
(12) 43p.		15a. DECLASSIFICATION/DOWNGRADING SCHEDULE

16. DISTRIBUTION STATEMENT (of this Report)

Distribution of this document is unlimited.

17. DISTRIBUTION STATEMENT (of the abstract entered in Block 20, if different from Report)

18. SUPPLEMENTARY NOTES

19. KEY WORDS (Continue on reverse side if necessary and identify by block number)

Bottom-type Recognition
Remote Sensing
Multispectral Scanner
Data Processing

20. ABSTRACT (Continue on reverse side if necessary and identify by block number)

A multichannel algorithm has been developed for bottom-type recognition under a variable depth of water. This algorithm is described, and the two-channel version of the algorithm is evaluated theoretically and empirically for several hypothetical and real situations. The radiative transfer model used for development and testing of this algorithm is also described, and an empirical verification of the model is presented.

DD FORM 1 JAN 73 1473 EDITION OF 1 NOV 65 IS OBSOLETE

UNCLASSIFIED

SECURITY CLASSIFICATION OF THIS PAGE (When Data Entered)

410 931

ACKNOWLEDGMENTS

The work which culminated in this report was carried out over a four year period, and involved the efforts of a number of ERIM staff members not mentioned in the report. The contributions of Dr. Robert Vincent, who initiated the contract, and Dr. Chester Wezernak, who guided work on the bottom features task during the first two years of the contract, are especially noted. Valuable discussions were also held with non-ERIM personnel, including Mr. James Slone, Mike Cooper, and Robert Arnone of the Naval Coastal Systems Center (NCSC). The continued guidance and comments of the technical monitor, Mr. Hans Dolezalek of the Office of Naval Research (ONR), is also gratefully acknowledged.

The relationship between the work described in this report and that carried out under contract with NCSC and other sponsors deserves some comment here. Progress in most scientific endeavors involves an interplay between theory and experiment, and the same is true of the progress reported here. In the work funded by ONR for the past four years, the emphasis has been on theoretical analysis of the basic relationships involved in optical remote sensing of shallow water areas. This analysis has resulted in benefits to other projects involving collection and processing of actual remote sensing data, and these projects have in turn stimulated and guided the theoretical work. ERIM's first involvement in the field of bottom-features mapping was in a project sponsored by the Environmental Protection Agency (EPA), and much of the stimulus for developments during the past two years has been provided by a series of experiments funded by NCSC. In fact, some of the material presented in the empirical evaluation section of this report has also appeared in reports to NCSC, although not with the same emphasis. Similarly, algorithms developed during this contract are expected to benefit efforts by the Defense Mapping Agency (DMA) to utilize satellite data for bathymetric purposes, and information gained from these DMA efforts has aided the ONR program. In this regard. our debt to

Mr. James Hammack and John Spinning of the DMA Hydrographic Center and Fabian Polcyn of ERIM is also acknowledged.

In the non-technical aspects of this project, we wish to thank Ms. Nancy Moon and Ms. Evelyn Wrabel for their efforts in typing and report preparation.

TABLE OF CONTENTS

LIST OF FIGURES

LIST OF TABLES

1
INTRODUCTION

This final report on Contract N0014-74-C-0273 summarizes work on the bottom features task during the four year period of this contract, concentrating especially on the fourth year results. A report on the beach environment task of this contract has been prepared under separate cover. The work was accomplished at the Environmental Research Institute of Michigan under the guidance of Principal Investigators Robert Vincent and later Fred Thomson. The performance period for this contract was January 1974 - February 1978.

This introduction contains a description of the bottom features task and a discussion of its relevance to the coastal reconnaissance problem. A summary of the accomplishments made during this contract is contained in Section 2, and a detailed technical discussion follows in Section 3.

The bottom features task arose from earlier research on water depth mapping using the selective penetration of light in water in various spectral bands as sensed by a passive multispectral scanner. Since the reflected light is influenced by both the water depth and the bottom type, these two problems are closely related. In the case of depth mapping, the object is to combine the signals in various wavelength bands in order to produce an output signal which varies only with depth, independently of the bottom type. Conversely, in the case of bottom features mapping the problem is to remove the effect of depth variations so as to produce a depth-invariant indicator of bottom type. It now appears that the bottom features problem is the prior one in the sense that bottom type information can be extracted without knowledge of depth, but depth information cannot be reliably extracted in the general case without knowledge of the bottom type.

Research on the extraction of water depth information from multispectral scanner data has been carried out at ERIM since 1967 under the

sponsorship of of various federal agencies including NASA, NOAA/NESS, and the Defense Mapping Agency. Techniques for extracting bottom-type information have also been studied at ERIM since 1972, first under the sponsorship of the Environmental Protection Agency and since 1974 for the Office of Naval Research. The specific purpose of the research sponsored by EPA was to map the distribution of Cladophora in Lake Ontario, while the efforts supported by ONR have been directed toward the general problem of mapping bottom features.

The relevance of the bottom features mapping task to the general coastal reconnaissance problem lies not only in its connection with depth mapping, but also in the information it can give about coastal geology and ecology. Information about the subsurface geology can sometimes be given directly (e.g., through differentiation of sand, rock, mud, coral, etc.) and sometimes indirectly through the association of benthic algal communities with different substrate types. Information about coral or algal communities is useful in ecological studies, relating to natural marine ecosystems and the impact of waste discharge, runoff, and resource extraction activities.

2

SUMMARY OF RESULTS AND RECOMMENDATIONS FOR FURTHER STUDY

The first work done at ERIM on the problem of bottom-features recognition was based on an analysis of imagery generated by an analog ratio processing technique, using multispectral data collected by ERIM aircraft over Lake Ontario and the east coast of Florida. The disadvantage of this technique was that the processing was not able to be precisely controlled and, therefore, was not repeatable. During the first year of the ONR program (1974) an analysis was carried out, using a simple water reflectance model, which resulted in the definition of a modified ratio algorithm (MRA) and the implementation of this algorithm on a digital computer. During the second year (1975) an investigation of the limitations of the MRA was begun using the simple radiance model, and a more accurate model incorporating the effects of scattering in the water was developed. In the third year (1976) the model was extended to include atmospheric effects, and a more thorough evaluation of the MRA was accomplished using this model. This analysis indicated certain basic limitations of the MRA and suggested a more general algorithm based on a logarithmic transformation of the radiance data collected by the scanner.

The limitations of the modified ratio algorithm are that (1) it is inherently a two-band technique, (2) the wavelength bands must be chosen carefully for each water type, such that the water attenuation coefficients are the same in both bands, and (3) the technique cannot discriminate between bottom types with equal reflectance ratios in these bands. As a result of these limitations, the average probability of correct classification for three typical bottom types (sand, mud, and vegetation) in clear coastal water (Jerlov Type 3) is only about 83% at zero water depth and falls to 50% at a depth of 6 meters for a typical aircraft scanner.

During the last year of this contract an improved bottom recognition algorithm was developed which is not subject to these limitations. This algorithm can utilize any number of bands, and the choice of these bands is not limited by the constraints imposed in the MRA. In fact, by choosing bands with different water attenuation coefficients, materials with similarly shaped reflectance spectra which could not be separated by the MRA can be discriminated using the new technique. The two-band version of this algorithm has undergone limited theoretical and empirical evaluations,which are the subject of this report. For the situation described above, the improvement in classification accuracy is shown in Figure 1.

A theoretical water reflectance model developed for the purpose of evaluating the bottom recognition algorithms has proved to be a valuable product of the ONR program in its own right. This model has been described in previous reports [1-3] and will also be reviewed in Section 3 of this report. The model has been used in various programs for the Navy [4] and the National Oceanic and Atmospheric Administration [5-7], and is planned for use in several new programs for NASA. The results accomplished during this contract may be summarized as follows:

1) Through a sequence of modeling and algorithm development steps, a multichannel algorithm has been developed for bottom type recognition, under a variable depth of water. The optimum channels for this algorithm are selected primarily on the basis of spectral differences in bottom type. The probability of correct classification for a typical situation using the latest algorithm and the previous algorithm (MRA) are shown in figure 1.

2) As an outgrowth of algorithm development, a radiative transfer model has been developed which is able to calculate the spectral radiance received by a sensor at any altitude, under arbitrary solar illumination, view angles, and atmospheric conditions, and for arbitrary water properties and bottom reflectances.

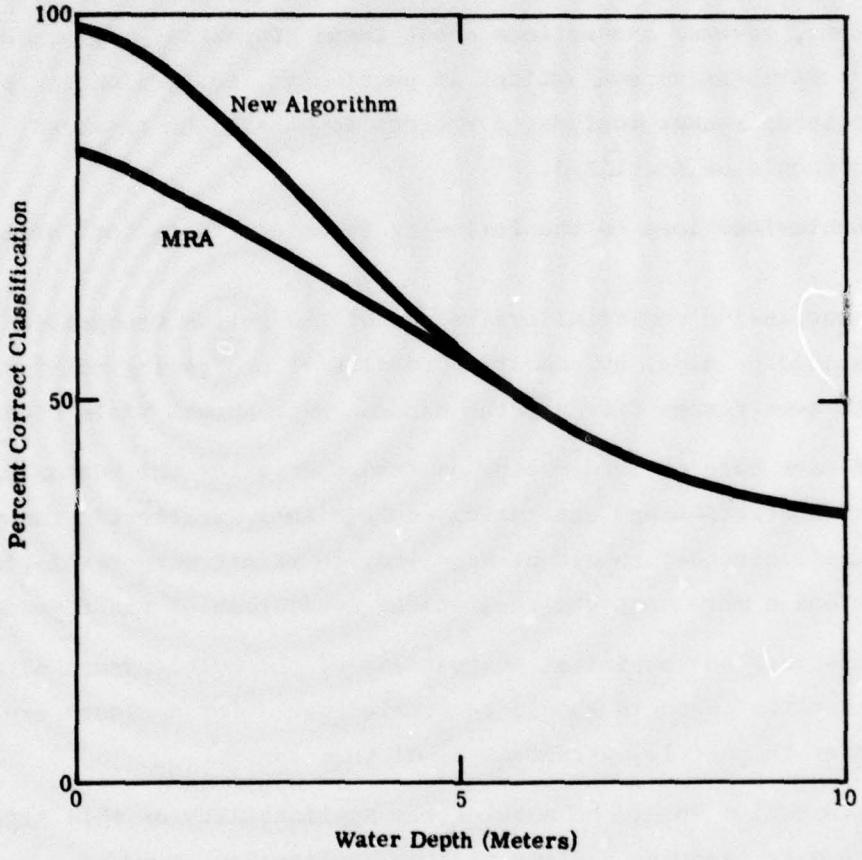

FIGURE 1. AVERAGE PROBABILITY OF CORRECT CLASSIFICATION OF THREE BOTTOM TYPES (SAND, MUD, AND VEGETATION) IN JERLOV WATER TYPE 3 USING NEW BOTTOM RECOGNITION ALGORITHM (UPPER CURVE) AND THE MODIFIED RATIO ALGORITHM (LOWER CURVE).

3) A comprehensive evaluation of the accuracy of the new algorithm requires knowledge of coastal water absorption, scattering, and scattering phase functions which is not presently available. Therefore, in evaluating the algorithms, several assumptions about these properties were made. For a more comprehensive evaluation, in particular, for evaluation of candidate coastal sensor designs, a program to obtain the required information should be initiated.

These conclusions lead to the following recommendations for further study:

1) A quantitative empirical evaluation of the bottom recognition algorithm should be made, by comparing results of processing multispectral scanner data over Panama City and the Bahamas with actual field conditions.

2) A broader base of information on important water and bottom parameters (i.e., water absorption and scattering coefficients, scattering functions, and bottom reflectances) should be acquired, to permit more realistic simulations and a more complete theoretical evaluation of the algorithm.

3) Theoretical and empirical evaluations of the multichannel algorithm with more than two channels should be carried out. For a closer explanation of this, refer to page 13, paragraph 2, of this report.

4) An evaluation should be made of the applicability of this algorithm to satellite data, and the utility of this application should be examined in view of the spectral channels and spatial resolution available with current satellites.

3

ALGORITHM DEVELOPMENT AND EVALUATION

This section contains a discussion of the bottom recognition algorithm developed during the fourth year of this contract, including the methods used for developing and evaluating the algorithm and the results of this evaluation. The theoretical water radiance model used in the development and evaluation of the algorithm is described in Section 3.1. The algorithm itself is described in Section 3.2, and the evaluation of the algorithm theoretically and empirically is discussed in Sections 3.3 and 3.4, respectively.

3.1 WATER RADIANCE MODEL

The water radiance model used for developing and evaluating the bottom recognition algorithm is a modification of the quasi-single-scattering approximation [8] which includes the effects of reflection from the bottom and from the air-water interface, as well as scattering and absorption in the water. This approximation has the advantage of computational speed over exact numerical methods, and gives results which are probably within the range of measurement accuracy. Comparisons with exact calculations were presented in an earlier report [1], and the results of an empirical test follow in this section.

An atmospheric model [9] was also combined with the water radiance model in order to fully simulate the radiance received at an airborne sensor. This atmospheric model is used to calculate the solar irradiance at the surface, the sky radiance, the path radiance, and the atmospheric transmittance. The total radiance at the sensor aperture is given by

$$L_{tot} = \left\{ n^2 T_s L(u', \phi) + r_s L_s \right\} T_a + L_p \qquad (3.1)$$

where n = index of refraction of water

T_s = transmittance of air-water interface

$L(\mu', \phi)$ = upwelling underwater radiance (c.f. Appendix, p. 33)

r_s = reflectance of air-water interface

L_s = sky radiance (from atmospheric model)

T_a = atmospheric transmittance (from atmospheric model)

L_p = path radiance (from atmospheric model)

An experiment conducted jointly by ERIM and the Naval Coastal Systems Center (NCSC)* in May 1977 [10] presented an opportunity for empirically evaluating the water/atmospheric model. In situ measurements were made of the reflectance of three bottom types in St. Andrew Bay, Florida, using an ISCO spectroradiometer and three known reflectance panels. Samples of bright sand from the Gulf of Mexico beach near Panama City, Florida were also taken and laboratory measurements were made of the reflectance of those samples at ERIM using a Cary-14 spectrometer. The measured reflectances for these four bottom types are shown in Figure 2. Water optical parameters were measured in situ by NCSC personnel, and determined independently by an analysis of the radiances measured by the ERIM M-8 airborne multispectral scanner. Diffuse attenuation coefficients for the Gulf and Bay waters determined by the latter procedure are shown in Figure 3. These values agree quite closely with the photometer measurements ($K = 0.15\text{-}0.25\ m^{-1}$ in Gulf, and $K = 0.35\text{-}0.45\ m^{-1}$ in Bay) made by NCSC [11]. Additional measurements of the beam attenuation coefficient (α) allowed an estimate of the total scattering coefficient (s) using the approximate relationship

$$s \approx \alpha - K \qquad (3.2)$$

This estimate of s was $0.5\ m^{-1}$ for the Gulf and $1.0\ m^{-1}$ for the Bay. Since the Bay presents the more interesting situation in terms of scattering and diverse bottom conditions, a set of radiances was

*Contract N61339-77-C-0059.

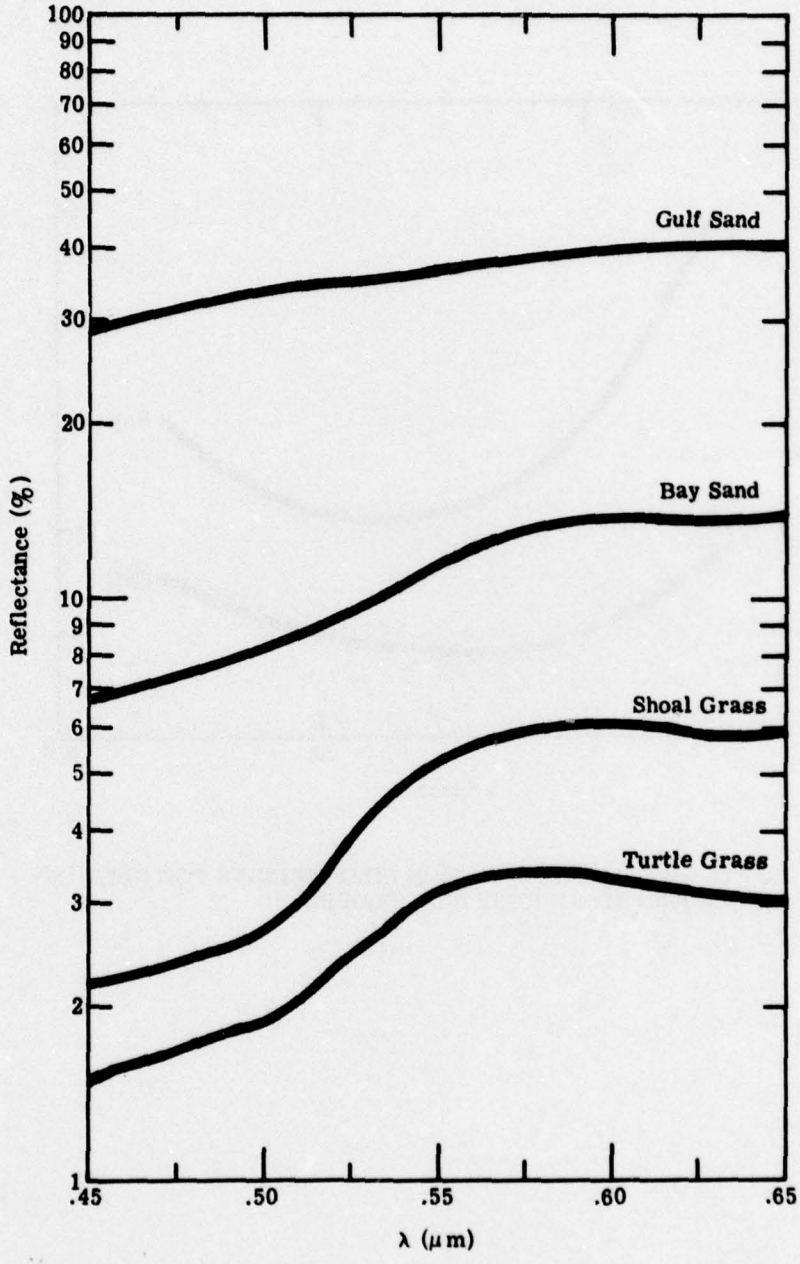

FIGURE 2. BOTTOM REFLECTANCES MEASURED AT PANAMA CITY, FLORIDA.

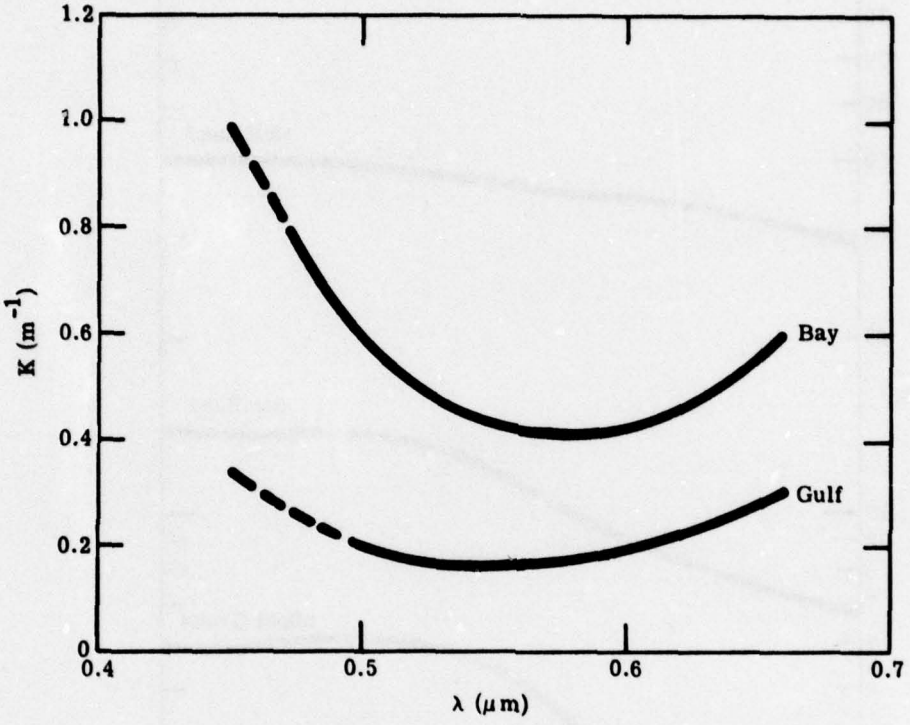

FIGURE 3. DIFFUSE WATER ATTENUATION COEFFICIENTS FOR GULF OF MEXICO AND ST. ANDREW BAY, FLORIDA.

calculated for the Bay using the parameters discussed above, and assuming an average particle scattering function from the measurements of Petzold [12]. The radiances were calculated for a water depth of 1 meter, and compared with radiances measured by the M-8 scanner at approximately the same depth. The comparison is shown in Figure 4. The only systematic difference between the calculated and measured values is in the blue region (.475-.50μm). It is not known whether this difference is due to errors in measurement of parameters, deficiencies in the model, or miscalibration of the scanner. However, the overall error is quite small and the comparison was considered to be a confirmation of the model.

3.2 BOTTOM RECOGNITION ALGORITHM

The bottom recognition algorithm is a technique for transforming a set of N variables (essentially the radiances in N wavelength bands) which contain both water depth and bottom type information into a set of N-1 depth-invariant variables containing only bottom type information, and one variable containing depth information. This process is actually a composite of two separate operations. The first operation is performed by subtracting the deep-water signal from each data point and taking the natural logarithm of the difference. The purpose of this step is to linearize the depth-dependence of the bottom-reflected signals. The water radiance model described in Section 3.1 shows that this linearization is only approximate, but that significant nonlinearities only occur for very bright bottoms and shallow depths. The second operation is a linear transformation which has the properties of a coordinate system rotation. The purpose of this transformation is to remove the depth dependence from all but one of the signal channels.

The mathematical formulation of this algorithm is detailed in the Appendix of this report for the general case of N channels. A method

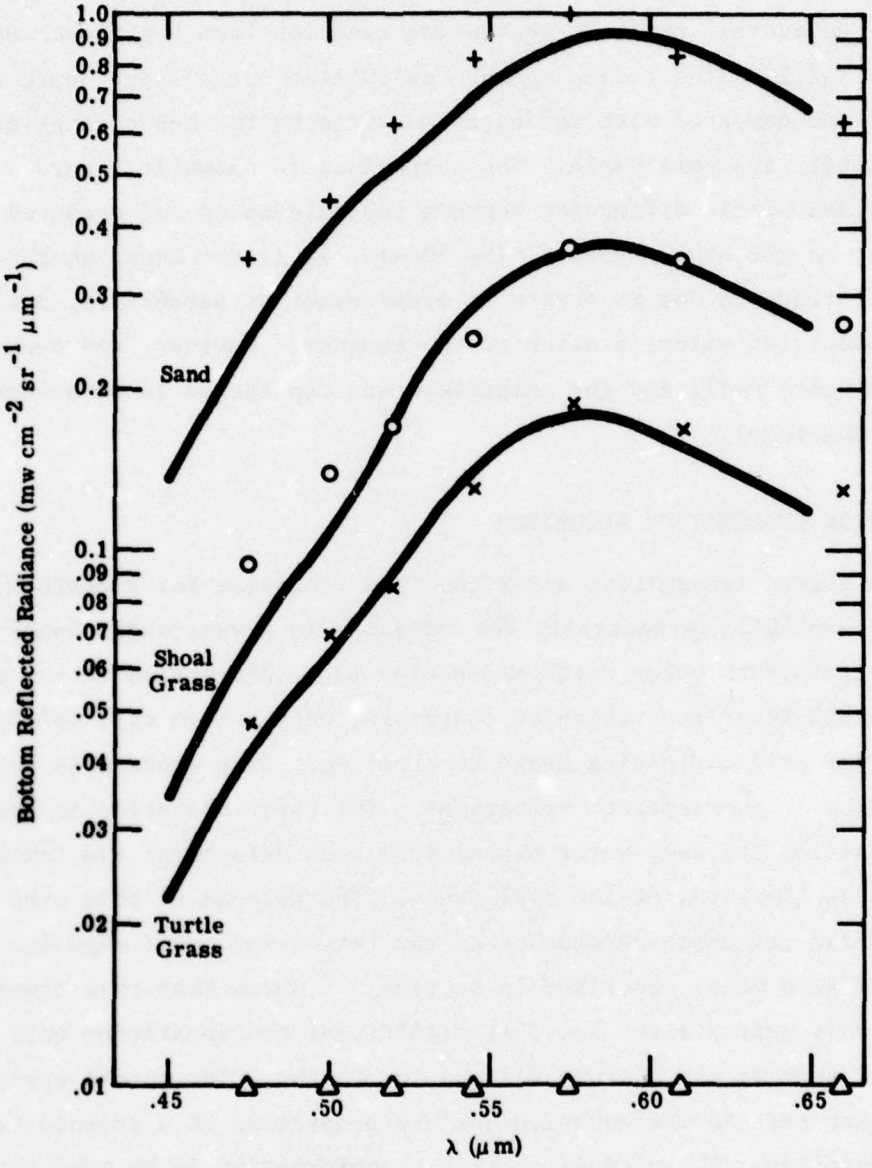

FIGURE 4. CALCULATED (CURVES) AND MEASURED (POINTS) RADIANCES FOR WATER DEPTH ≈ 1 METER, ST. ANDREW BAY, FLORIDA.

of evaluating the performance of the algorithm for the two-channel case is also described in the Appendix, and results are presented for one specific case. Further results are presented in Section 3.3., including a determination of optimum bands for three different water and bottom types.

For the two-band case the algorithm results in a single depth-invariant variable which may be used as an index of the bottom type. For the case of three or more input bands, the algorithm results in two or more depth-invariant channels. Thus, a further step is required to combine this information into a single index of bottom type. Such multivariate pattern recognition techniques exist, but they have not as yet been combined with the algorithms described in this report. Consequently only the two-band case has been fully implemented and evaluated. It is expected that the addition of a third band will yield a small but possibly significant improvement in classification accuracy, and that the incremental improvements for more than three bands will decrease with the number of bands employed.

3.3 THEORETICAL EVALUATION

A computer program was written to perform an error analysis for the two-channel bottom recognition algorithm, using the radiance model described above to simulate the data collected by a multispectral scanner system. The program considers all possible pairs of the wavelength bands entered and computes the probability of misclassification for each bottom type at each depth entered.

For each wavelength pair, the program calculates the coordinate system rotation parameters as described in the Appendix using the known water attenuation coefficients. The values of Y_1 (the depth-invariant variable) are calculated at the "training depth" for each bottom type, and the decision boundaries are chosen midway between the neighboring values of Y_1.

After the "training" process is completed, the radiance data is read again and the probability of classification in each category is calculated for the value of NEΔL (the noise-equivalent radiance) entered. The results for sand, mud,

and vegetation in Jerlov's [13] water type 3 are reported in the Appendix for a noise figure NEΔL = .05 mW cm^{-2} sr^{-1} μm^{-1}. This value is typical for an aircraft scanner such as the ERIM M-7 and M-8 scanners, but may be improved by techniques such as spatial filtering or by changes in system design. In the 1977 NCSC experiment [14] the noise was reduced to approximately .02 mW cm^{-2} sr^{-1} μm^{-1} by applying a 3 x 3 pixel smoothing function to the data collected by the M-8 scanner.

The error analysis was repeated for each possible wavelength pair in the range 0.4-0.6μm with 0.025μm intervals, using the lower noise figure. The results for water type 3 are shown in tables 1 and 2 for depths of 2 meters and 4 meters, respectively. These results were obtained using a training depth of 2 meters.

The results shown in tables 1 and 2 reveal two distinct regions where the performance is optimized. The band pair .475-525μm is representative of the first region and the band pair .525-.60μm is representative of the second region. Although the second band pair gives slightly better results at 2 meters, the first band pair has the advantage of being less sensitive to changes in water quality. Figure 5 shows the average percent correct classification for the band pair .475-525μm as a function of depth in water type 3, assuming the algorithm has been trained in this water type at 2 meters depth, and the performance in Jerlov's water type 5 with the same operating parameters. Thus, the algorithm correctly classifies the bottom about 80% of the time in water type 3 at 4 meters depth, but if a portion of the scene contains water type 5, the classification accuracy for this portion drops to about 50% at a depth of 4 meters.

TABLE 1

AVERAGE CLASSIFICATION ACCURACY FOR SAND, MUD, AND VEGETATION IN WATER TYPE 3 AT 2 METERS DEPTH

BAND 1 WAVELENGTH	.45	.475	.50	.525	.55	.575	.60	.625	.65
.45	33								
.475	77	33							
.50	77	59	33						
.525	97	97	71	33					
.55	97	95	77	46	33				
.575	62	70	72	99	98	33			
.60	61	68	93	99	99	70	33		
.625	62	83	96	97	97	81	63	33	
.65	72	89	95	96	97	70	61	61	33

BAND 2 WAVELENGTH

TABLE 2

AVERAGE CLASSIFICATION ACCURACY FOR SAND, MUD, AND VEGETATION IN WATER TYPE 3 AT 4 METERS DEPTH

BAND 1 WAVELENGTH	.45	.475	.50	.525	.55	.575	.60	.625	.65
.45	33								
.475	50	33							
.50	55	45	33						
.525	73	82	66	33					
.55	71	78	68	39	33				
.575	42	51	57	81	78	33			
.60	41	51	62	82	81	46	33		
.625	41	51	57	72	71	47	39	33	
.65	47	48	52	69	68	44	39	38	33

BAND 2 WAVELENGTH

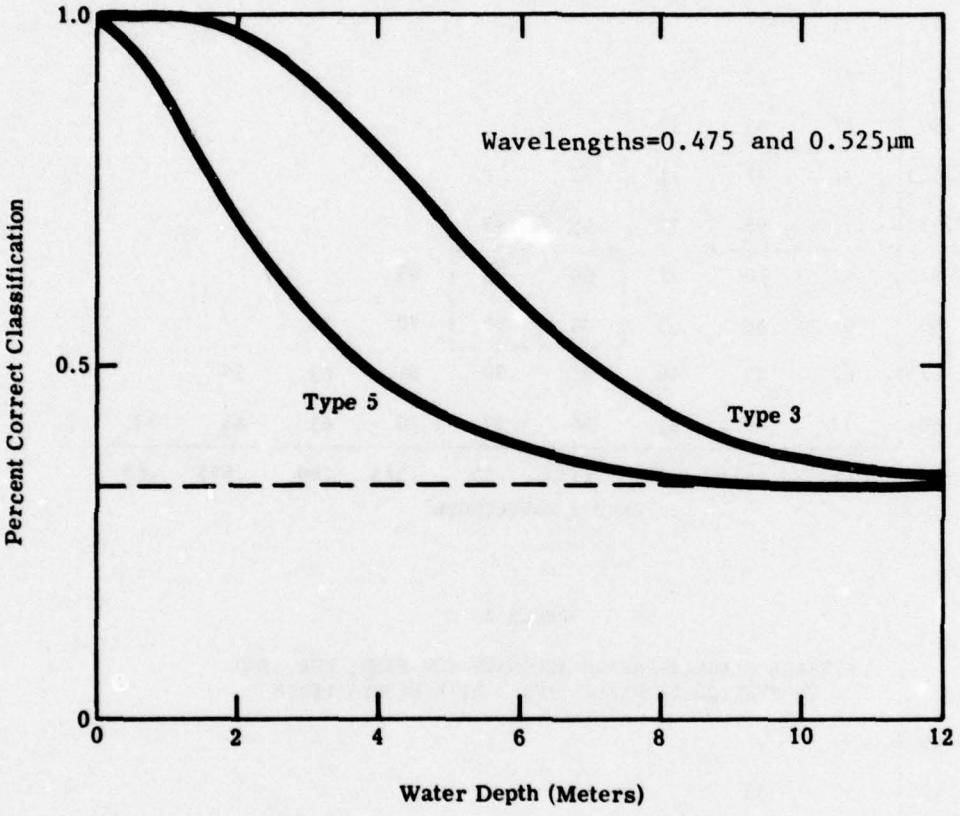

FIGURE 5. AVERAGE PROBABILITY OF CORRECT CLASSIFICATION OF SAND, MUD, AND VEGETATION IN WATER TYPES 3 AND 5, FOR BOTTOM RECOGNITION ALGORITHM TRAINED IN WATER TYPE 3 AT 2 METERS DEPTH.

Similar calculations were carried out for water type 5, training the algorithm in this water type at 2 meters depth. The results of these calculations are shown in tables 3 and 4. The optimum wavelength pairs seem to be very nearly the same for this case, suggesting that the optimum wavelengths are determined primarily by the bottom types rather than by the water type. The decision boundaries selected for water type 5 are similar to those for water type 3 in the first group (around .475-.525μm) but are quite dissimilar in the second group (around .525-.60μm). This accounts for the relative insensitivity of the algorithm to changes in water quality using the first wavelength pair, and the large sensitivity using the second wavelength pair. Figure 6 shows the performance of the algorithm trained in water type 5, using the band pair .475-.525μm, and evaluated for water type 5 and water type 3.

A simulation was also done for the St. Andrew Bay test site, with sand, shoal grass, and turtle grass as the bottom types. The water attenuation coefficients at this site (c.F. Figure 3) were intermediate between Jerlov types 5 and 7. The algorithm was trained at 1 meter and evaluated at 1 and 2 meters for each wavelength pair. These results are shown in tables 5 and 6. The optimum bands for this case appear to be .575-.65 μm or .60-.65 μm. These are very close to the actual M-8 bands selected for processing the St. Andrew Bay data set during the 1977 NCSC experiment [14]. The performance using the .60-.65 μm band pair is shown in Figure 7 for sand only (upper curve),and averaged over all three bottom types (lower curve). The average probability of correct classification is smaller in this case than for water type 5 (Figure 6) because of the similarity of the reflectance spectra of shoal grass and turtle grass, and because of the greater attenuation of the water. When only a discrimination between sand and vegetation is attempted, the probability of correct classification is much higher, as shown in the upper curve of Figure 7.

TABLE 3

AVERAGE CLASSIFICATION ACCURACY FOR SAND, MUD, AND VEGETATION IN WATER TYPE 5 AT 2 METERS DEPTH

BAND 1 WAVELENGTH	.45	.475	.50	.525	.55	.575	.60	.625	.65
.45	33								
.475	56	33							
.50	62	54	33						
.525	78	93	81	33					
.55	78	92	74	41	33				
.575	60	59	47	90	86	33			
.60	70	50	78	97	96	82	33		
.625	61	74	82	99	99	89	51	33	
.65	73	80	82	97	98	89	66	53	33

BAND 2 WAVELENGTH

TABLE 4

AVERAGE CLASSIFICATION ACCURACY FOR SAND, MUD, AND VEGETATION IN WATER TYPE 5 AT 4 METERS DEPTH

BAND 1 WAVELENGTH	.45	.475	.50	.525	.55	.575	.60	.625	.65
.45	33								
.475	36	33							
.50	38	37	33						
.525	42	53	53	33					
.55	41	52	52	35	33				
.575	37	39	37	55	54	33			
.60	38	36	44	63	61	46	33		
.625	39	41	46	59	58	47	36	33	
.65	39	41	45	54	53	45	39	36	33

BAND 2 WAVELENGTH

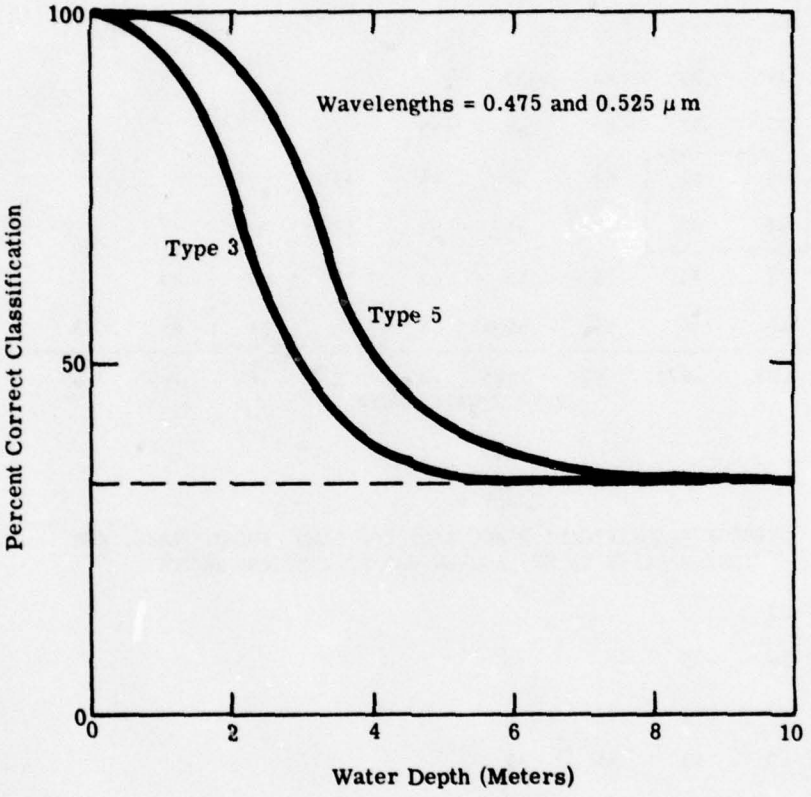

FIGURE 6. AVERAGE PROBABILITY OF CORRECT CLASSIFICATION OF SAND, MUD, AND VEGETATION IN WATER TYPES 3 AND 5, FOR BOTTOM RECOGNITION ALGORITHM TRAINED IN WATER TYPE 5 AT 2 METERS DEPTH.

TABLE 5

AVERAGE CLASSIFICATION ACCURACY FOR SAND, SHOAL GRASS, AND TURTLE GRASS IN ST. ANDREW BAY AT 1 METER DEPTH

BAND 1 WAVELENGTH	.45	.475	.50	.525	.55	.575	.60	.625	.65
.45	33								
.475	52	33							
.50	66	63	33						
.525	74	73	64	33					
.55	77	77	69	48	33				
.575	80	81	67	51	46	33			
.60	81	82	70	54	51	47	33		
.625	77	75	74	55	41	56	61	33	
.65	66	54	51	56	68	76	81	68	33

BAND 2 WAVELENGTH

TABLE 6

AVERAGE CLASSIFICATION ACCURACY FOR SAND, SHOAL GRASS, AND TURTLE GRASS IN ST. ANDREW BAY AT 2 METERS DEPTH

BAND 1 WAVELENGTH	.45	.475	.50	.525	.55	.575	.60	.625	.65
.45	33								
.475	36	33							
.50	40	42	33						
.525	40	43	44	33					
.55	41	44	49	39	33				
.575	41	46	51	39	38	33			
.60	42	46	53	40	40	39	33		
.625	40	43	51	41	36	42	44	33	
.65	38	37	39	44	50	55	57	48	33

BAND 2 WAVELENGTH

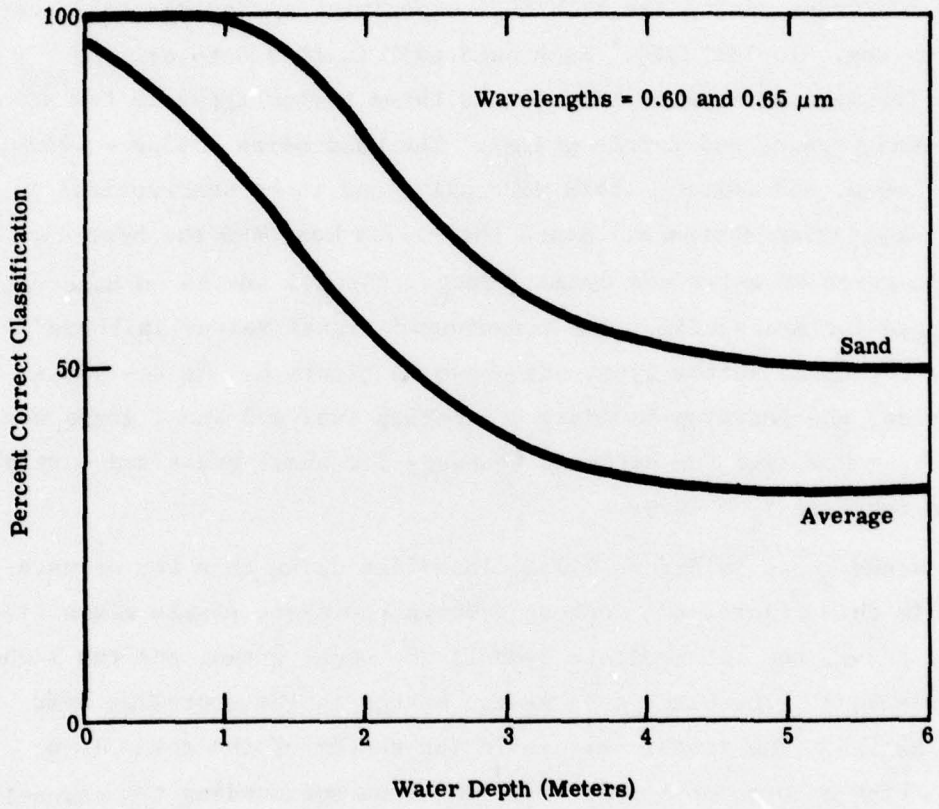

FIGURE 7. AVERAGE PROBABILITY OF CORRECT CLASSIFICATION OF SAND, SHOAL GRASS, AND TURTLE GRASS (LOWER CURVE), AND PROBABILITY OF CORRECT CLASSIFICATION OF SAND ONLY (UPPER CURVE) FOR ST. ANDREW BAY, FLORIDA. TRAINING DEPTH = 1 METER.

3.4 EMPIRICAL EVALUATION

The two-channel bottom recognition algorithm has been applied to two actual data sets. The first application was to the data set collected by the M-8 scanner during the ERIM/NCSC experiment on May 26, 1977 over St. Andrew Bay, Florida [14].* Each band pair in this data set was examined for maximum separability of the three bottom types in the scene (sand, shoal, grass, and turtle grass). The band pairs .545μm - .66μm, .575μm - .66μm, and .61μm - .66μm were all found to be near-optimal in terms of separation distance. Since the .545μm band had the best data quality in terms of noise and dynamic range, the .545 μm-.66 μm band pair was selected for processing. The transformed signal values in these bands for the three bottom types are shown in Figure 8. On the basis of this plot, the decision boundary separating sand and shoal grass was taken as $Y_1 = 0.0$, and the decision boundary for shoal grass and turtle grass was taken as $Y_1 = -0.4$.

The scene shown in Figure 9 was classified using this set of parameters. In this figure, the darkest symbols represent pixels classified as turtle grass, the intermediate symbols are shoal grass, and the lightest symbols are sand. The blank area at the bottom is the shoreline near the NCSC Marina. The linear feature in the center of the scene is a channel having a depth of 4-5 meters. The area surrounding the channel has a depth of 1-2 meters, dropping off rapidly to 5-6 meters at the top of the scene. The dimensions of the scene are approximately 320 meters in each direction (there is some distortion of scale in the line printer display). An aerial photograph of the scene is shown in Figure 10 for comparison.

The sandy areas near the shoreline, in scattered patches, and on the steep slopes of the channel (center of scene) and at the edge of the bank (top of scene) appear to be correctly classified. The zones of shoal grass in the center and of turtle grass near the top of the bank appear

*Data collection and processing for this experiment were carried out under contract with NCSC, contract no. N61339-77-C-0059.

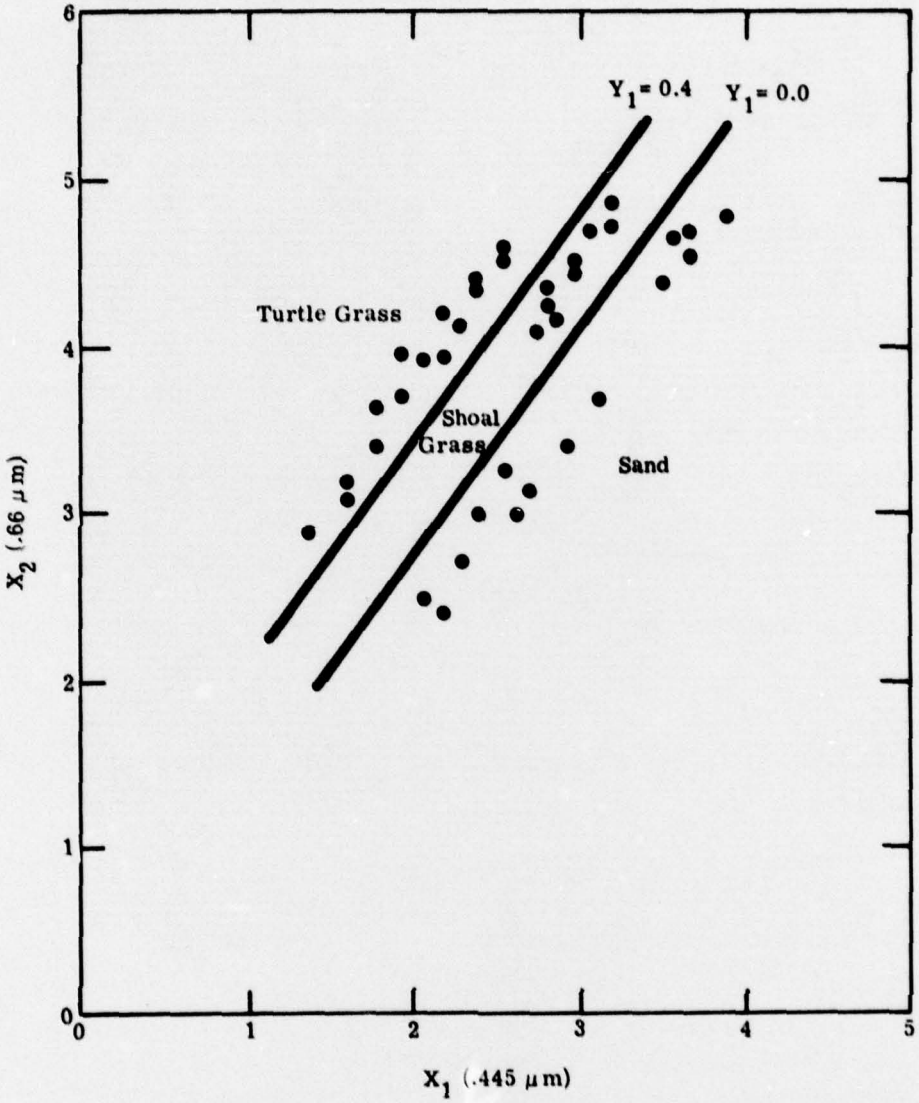

FIGURE 8. TRANSFORMED SIGNAL VALUES OVER THREE BOTTOM TYPES IN ST. ANDREW BAY, FLORIDA

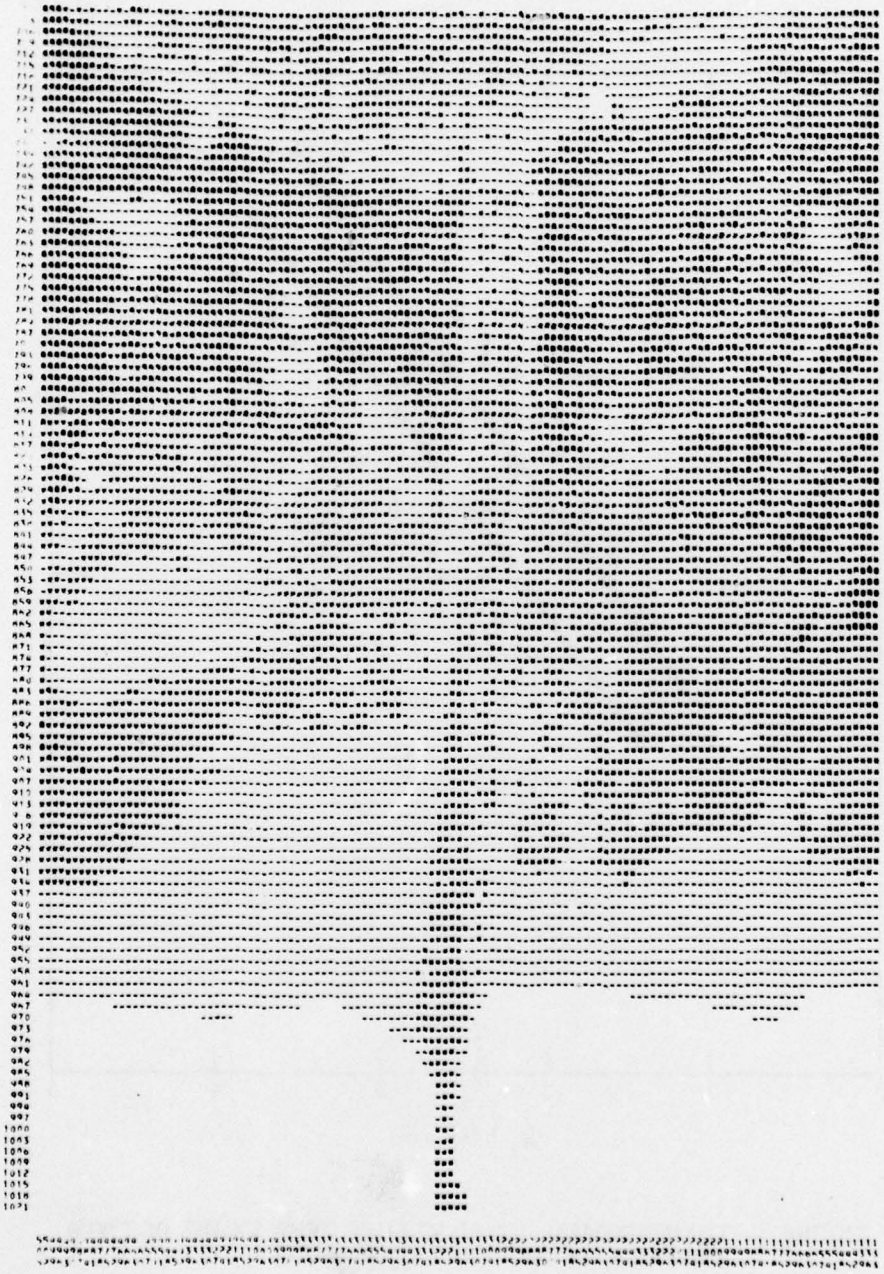

FIGURE 9. BOTTOM-TYPE MAP FOR ST. ANDREW BAY, FLORIDA.

FIGURE 10. AERIAL PHOTOGRAPH OF ST. ANDREW BAY TEST SITE

also to be generally correct. The classification as shoal grass in the center of the channel and in deep water at the top of the scene is more doubtful. A complete evaluation, utilizing subsurface observations made by NCSC personnel at the time of the overflight, would be desirable (see recommendations for further study, p. 6).

The second application of the bottom recognition algorithm was to Landsat data over the Bahamas. A high gain Landsat frame (5249-14435) over the Great Bahama Bank was selected for analysis. This data set had been previously used for bathymetric studies in a contract with the Defense Mapping Agency,* and covers an area which is currently under intensive study as a test range for development of satellite bathymetry techniques. One especially interesting part of the scene is a long linear feature just north of Mackie shoal, at about 25°40'N and 78°40'W. This previously uncharted feature was visited during a field trip in October 1977, and was found to consist of a sharp depth discontinuity of about 2 meters, with a heavy growth of turtle grass on the deeper (west) side and sand on the shallow (east) side. A plot of Landsat data values in MSS-4 (.50-.60μm) and MSS-5 (.60-.70μm) over both bottom types is shown in Figure 11. Assuming mean oceanic water attenuation coefficients, the decision boundary between sand and turtle grass is about $Y_1 = 3.0$.

A portion of this linear feature, including the southern terminus, is shown in Figure 12. The dimensions of this scene are about 6.9 km in width (left to right) by 8.3 km in length (top to bottom). This area was processed with the bottom recognition algorithm using mean oceanic water parameters. Darker symbols represent lower values of Y_1 and apparently correspond with heavier growths of turtle grass. Lighter symbols represent higher values of Y_1 and apparently correspond with sandy areas in the scene. Further analysis and evaluation of this scene is recommended to determine the accuracy and depth limits of the bottom recognition algorithm as applied to Landsat data.

*Contract number DMA-800-76-C-0057.

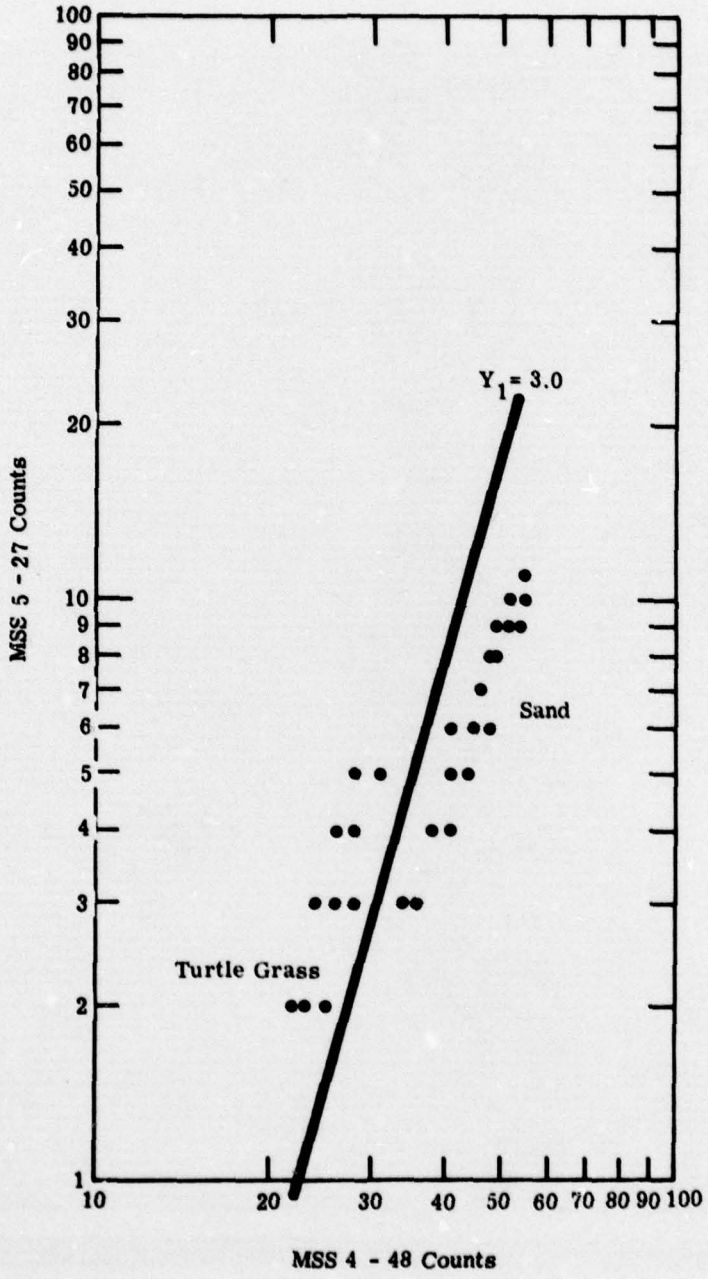

FIGURE 11. LANDSAT DATA VALUES OVER SAND AND TURTLE GRASS NEAR MACKIE SHOAL IN GREAT BAHAMA BANK.

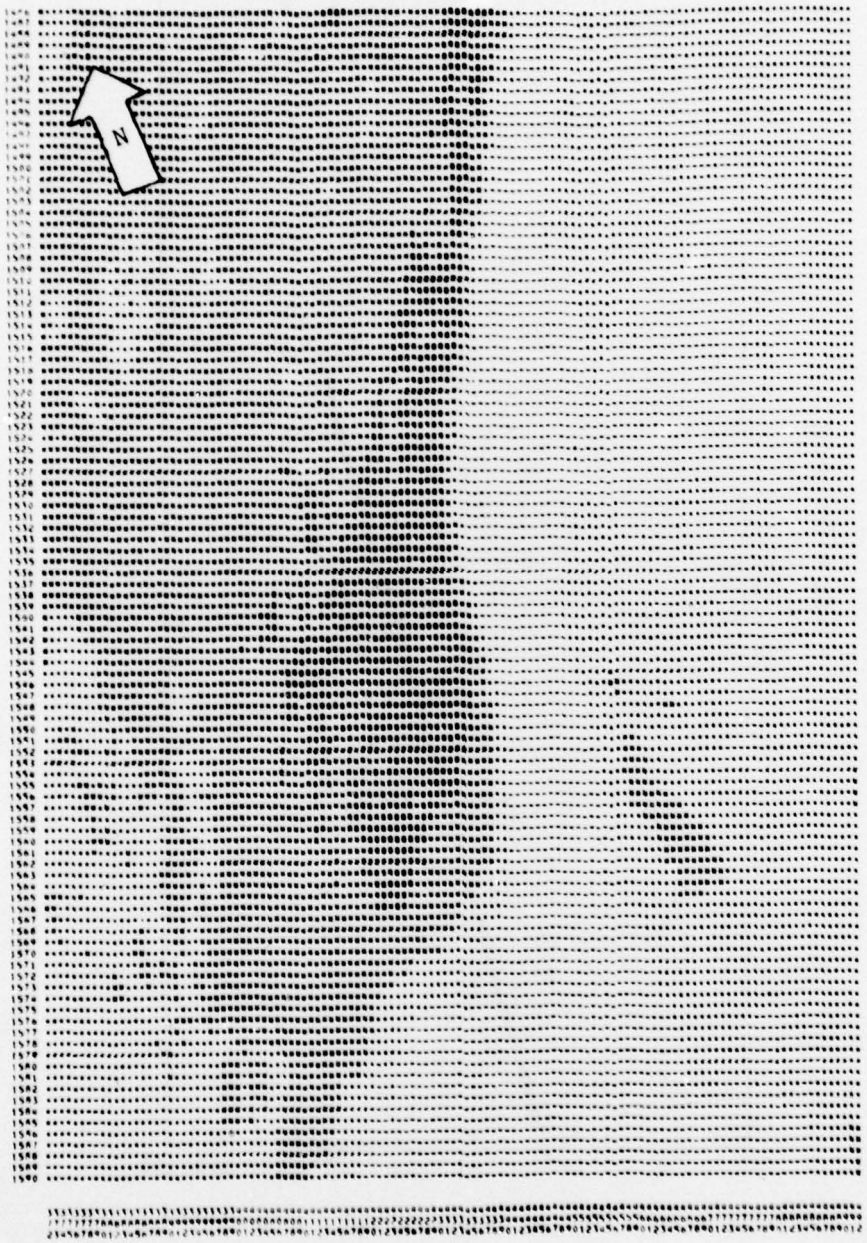

FIGURE 12. BOTTOM-TYPE MAP FOR MACKIE SHOAL, GREAT BAHAMA BANK.

Reprinted from APPLIED OPTICS, Vol. 17, page 379, February 1, 1978

APPENDIX

Passive remote sensing techniques for mapping water depth and bottom features

David R. Lyzenga

Ratio processing methods are reviewed, and a new method is proposed for extracting water depth and bottom type information from passive multispectral scanner data. Limitations of each technique are discussed, and an error analysis is performed using an analytical model for the radiance over shallow water.

Introduction

Aerial photography of shallow water areas can provide useful qualitative information on bottom composition, the distribution of benthic algal or coral communities, and water depth. However, the interpretation of this photography is impeded by the fact that water depth variations are not easily distinguished from bottom color differences. Surface reflection effects add another element of confusion to the interpretation of the photography. The use of digitally recorded multispectral scanner data permits corrections to be made for surface reflection effects and also allows the possibility of automatic recognition of bottom features and water depth using radiometric techniques. Past research efforts have resulted in the development of specific techniques for each of these applications.[1,2] The purpose of this paper is to discuss the limitations of these techniques and to present a more general set of algorithms for both applications.

Ratio Algorithms

The techniques described in Refs. 1 and 2 were developed on the basis of a simple water reflectance model which accounts for the major part of the signal received by a multispectral scanner over clear shallow water, but neglects the effects due to scattering in the water and internal reflection at the water surface. According to this model, the radiance in a given wavelength band (i) can be written as

$$L_i = L_{si} + k_i r_{Bi} \exp(-\kappa_i f z), \tag{1}$$

where L_{si} is the radiance observed over deep water (due to external reflection from the water surface and scattering in the atmosphere); k_i is a constant which includes the solar irradiance, the transmittance of the atmosphere and the water surface, and the reduction of the radiance due to refraction at the water surface; r_{Bi} is the bottom reflectance; κ_i is the effective attenuation coefficient of the water; f is a geometric factor to account for the pathlength through the water; and z is the water depth.

The simplest method of extracting water depth information from multispectral scanner data is to invert Eq. (1) for a single wavelength band. An extension of this method would be to calculate the depth from two or more bands and average the results. The difficulty with this technique is, of course, that changes in the bottom reflectance or water attenuation cause errors in the depth calculation.

The water depth algorithm developed by Polcyn *et al.*[1] relies on the assumption that a pair of wavelength bands can be found such that the ratio of the bottom reflectances in these two bands is the same for all the bottom types within a given scene. That is, for bottom types $A, B, \ldots,$

$$\frac{r_{A1}}{r_{A2}} = \frac{r_{B1}}{r_{B2}} = \ldots = R_b, \tag{2}$$

where r_{A1} is the reflectance for bottom type A in band 1 etc. The water depth can then be calculated from the equation

$$z = \frac{1}{(\kappa_1 - \kappa_2)f}\left[\ln\left(\frac{k_1}{k_2}\right) - \ln\left(\frac{R}{R_b}\right)\right], \tag{3}$$

where R is the ratio of the bottom-reflected signals in the two bands:

$$R = (L_1 - L_{s1})/(L_2 - L_{s2}). \tag{4}$$

If the assumption expressed by Eq. (2) is correct, the depth calculated by this method is not affected by changes in bottom composition in the scene. The depth is also insensitive to changes in water quality if the

The author is with Environmental Research Institute of Michigan, P.O. Box 618, Ann Arbor, Michigan 48107.
Received 8 June 1977.
0003-6935/78/0201-0379$0.50/0.

difference between the attenuation coefficients ($\kappa_1 - \kappa_2$) remains constant. In many cases a pair of wavelengths can be found for which Eq. (2) is approximately satisfied, or for which ($\kappa_1 - \kappa_2$) remains relatively constant. However, the wavelengths which satisfy one criterion are in general not the same as those which satisfy the other, and if changes in bottom composition or water quality are too large, a pair of wavelengths may not exist which satisfies either criterion. Nevertheless, this method has been used with some success for extracting water depths from both satellite and aircraft multispectral scanner data over relatively clear water to a depth of approximately one attenuation length.[3,4]

The inverse problem is to extract information about the bottom reflectance (or bottom composition) from the radiance measured by the multispectral scanner. An algorithm was developed for this purpose[2] by noting that the radiance ratio R should be independent of the water depth if the effective water attenuation coefficients are the same in both bands. From the simple water reflectance model described above, this ratio then reduces to

$$R = (k_1 r_{B1})/(k_2 r_{B2}), \tag{5}$$

which may be used as an index of the bottom type, provided that the bottom types to be mapped have different reflectance ratios in the wavelength bands selected.

This method was successfully used for mapping the distribution of *Cladophora* (a green benthic algae) under a variable depth of water along the Lake Ontario shoreline.[2] The primary reason for the success of this application was the fact that the vegetation reflectance has distinctive features (due to chlorophyll absorption) in the blue–green region of the spectrum where the water attenuation is at a minimum. Thus it was possible to choose two bands with equal water attenuation coefficients and different bottom reflectance ratios for the green vegetation and the sand background.

In attempting to apply this method to a larger number of water types and bottom materials, however, several difficulties arose. First, the requirement of equal water attenuation coefficients in the operating wavelength bands causes operational difficulties, since the band positions must be changed when operating in different water types. Second, the requirement of different bottom reflectance ratios restricts the number of bottom materials that can be recognized, since materials with similarly shaped reflectance spectra (such as sand and mud) have nearly equal reflectance ratios. Finally, both ratio methods for bottom features and water depth are inherently restricted to two operating wavelength bands. Since independent information relating to both water depth and bottom composition can be collected simultaneously in several wavelength bands, methods which use only two of these bands do not make full use of the available information.

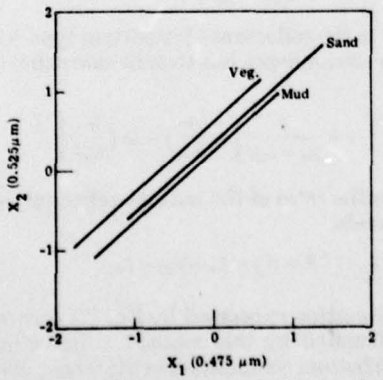

Fig. 1. Plot of X_1 vs X_2 for water type 3 with three bottom types. Water depth ranges from 0 m to 5 m on each curve.

More General Algorithms

In order to develop a more general set of algorithms for water depth and bottom features, the simple radiance model described above was modified to include the effects of scattering in the water and internal reflection at the water surface (see Appendix A). Examination of this model shows that the scattering term has the same depth dependence as the bottom-reflected radiance. Except for the effects of internal reflection, therefore, the total radiance for the case of direct incident radiation may be written in the same form as Eq. (1), with the actual bottom reflectance replaced by an apparent bottom reflectance

$$r_B' = r_B - \frac{\pi\beta(\mu_s)}{K(\mu + \mu')}. \tag{6}$$

The variables on the right-hand side of this equation are defined in Appendix A. This exponential depth dependence suggests the use of the transformation

$$X_i = \ln(L_i - L_{si}), \tag{7}$$

where L_{si} is the deep-water radiance (including scattering). The purpose of this transformation is to linearize approximately the relationship between the transformed radiances and the water depth. The nonlinearities which remain are caused by internal reflection effects, which are significant only for very shallow water and high bottom reflectances.

A plot of the transformed radiances over three bottom types at wavelengths of 0.475 μm and 0.525 μm is shown in Fig. 1. The water parameters used in this example are a composite of Jerlov's[5] irradiance attenuation coefficients for coastal water type 3 and Petzold's[6] scattering parameters for Station 5 off the coast of southern California. The irradiance attenuation coefficients were 0.223 m^{-1} and 0.198 m^{-1}, and the total scattering coefficient was 0.275 m^{-1} at the wavelengths used. In the absence of reliable reflectance measurements for actual bottom materials, the reflectances of beach sand, dark soil (representing mud), and wheat leaves (representing aquatic vegetation) were used for this calculation. These reflectances are plotted in Fig.

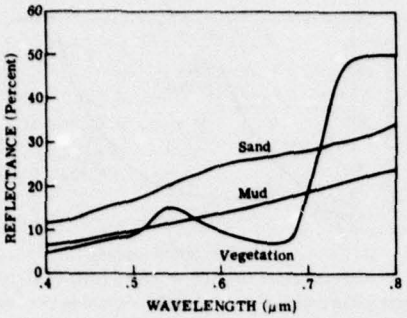

Fig. 2. Spectral reflectances of sand, mud, and green vegetation.

2. For these water and bottom parameters, the radiance due to scattering is equal to the bottom-reflected radiance at a depth of about 6 m.

Figure 1 represents a simulated data set for an ideal measurement situation with no noise and no variation in water or bottom parameters. For an actual data set, the data points would be randomly distributed about the lines in Fig. 1. Except for the slight curvature caused by internal reflection effects, the transformed radiance values over different bottom types describe parallel lines in X_i-space as the water depth varies continuously.

For an N-band system, the transformed radiances fall along a set of parallel lines in N-space. Thus, a second set of variables

$$Y_i = \sum_{j=1}^{N} A_{ij} X_j \tag{8}$$

can be obtained by rotating the coordinate system so that the Y_N axis is parallel to this direction (see Appendix B). If the linear transformation (8) is a pure rotation, only Y_N will be dependent on the water depth, while all the other variables are functions only of the bottom reflectance. For an N-band system, this results in a set of $N-1$ depth-invariant signals which can be used as inputs to a conventional maximum likelihood classification algorithm. The remaining variable can be written as

$$Y_N = B_m - Cz, \tag{9}$$

where B_m is a function of the bottom composition and C depends only on the water attenuation coefficients. If the bottom material can be recognized by the procedure outlined above, and the value of B_m determined for each bottom type, Eq. (9) can then be used to calculate the water depth.

Although this analysis bears a superficial resemblance to principal component analysis,[7] the only actual similarity is the use of a rotation transformation. In the case of principal component analysis, the first coordinate axis is aligned in the direction of maximum sample variance, and the remaining axes are aligned in the orthogonal directions with decreasing sample variance. The purpose of the principal component analysis as applied to water color[8] is to reduce the number of variables, since only a few of the principal components are usually needed to account for most of the sample variance. In the analysis presented here, the directions of the transformed coordinate axes are not necessarily related to the sample variance, and the purpose of the analysis is not to reduce the number of variables but to remove the depth dependence from all but one variable.

For a two-band system, the decision rule for bottom classification reduces to a simple test on the value of Y_1. That is, the bottom is classified as material m if

$$Y_{m1} < Y_1 < Y_{m2}, \tag{10}$$

where Y_{m1} and Y_{m2} are the lower and upper decision boundaries, respectively, for material m. If the radiances over a given bottom type m are assumed to be normally distributed (due to system noise) with mean value $\bar{L}_{im}$ and standard deviation $(NE\Delta L)_i$ in band i, the probability that this material will be classified as material n is approximately

$$P(m,n) = \tfrac{1}{2}\,\mathrm{erf}\left(\frac{d_1}{\sqrt{2}}\right) - \tfrac{1}{2}\,\mathrm{erf}\left(\frac{d_2}{\sqrt{2}}\right), \tag{11}$$

where

$$d_1 = (\hat{Y}_m - Y_{n1})/\sigma_m, \tag{12}$$

$$d_2 = (\hat{Y}_m - Y_{n2})/\sigma_m, \tag{13}$$

$$\sigma_m^2 = \sum_{i=1}^{2} A_{1i}^2 (NE\Delta L_i)^2/(\bar{L}_i - L_{si})^2. \tag{14}$$

The total probability of misclassification for material m is

$$\bar{P}(m) = 1 - P(m,m). \tag{15}$$

The total probabilities of misclassification for the three materials in Fig. 1 are plotted vs depth in Fig. 3 for $NE\Delta L = 0.05$ mW cm^{-2} sr^{-1} μm^{-1}.

It can be shown that for the case of two bands with equal attenuation coefficients, the method described above is equivalent to the ratio method. However, in this case the performance of both methods is worse than that shown in Fig. 3 because of the similar reflectance

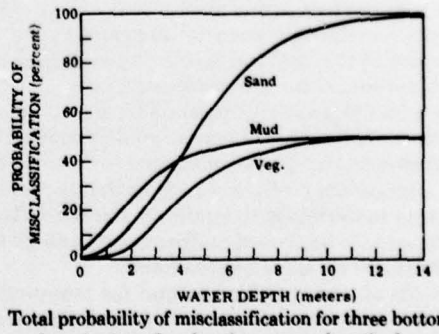

Fig. 3. Total probability of misclassification for three bottom types in water type 3, using the proposed method.

ratios of sand and mud. Thus, the performance of the ratio method can always be equaled and can usually be exceeded by the use of the proposed method with a more optimum pair of wavelengths. Further improvement in bottom classification would be expected if more than two bands were used.

After the bottom classification has been performed, the water depth can be calculated from Eq. (9), using the appropriate value of B_m for material m. Depth errors arise from the variance of Y_N due to noise, which is approximately given by

$$(\Delta Y_N)^2 = \sum_{i=1}^{N} A_{Ni}^2 (NE\Delta L_i)^2 / (L_i - L_{si})^2 \tag{16}$$

and from errors in bottom classification. Thus the total rms depth error for bottom type m is

$$\Delta Z_m = \frac{1}{C}\left[(\Delta Y_N)^2 + \sum_n P(m,n)(B_m - B_n)^2 \right]^{1/2}. \tag{17}$$

The average depth error for the three bottom types in water type 3 is plotted vs depth in Fig. 4. For comparison, the depth error due to noise only using the ratio method is also plotted in Fig. 4. The rms depth error due to noise for the ratio method is given by

$$\Delta Z_r = \frac{1}{(\kappa_1 - \kappa_2) f}\left[\left(\frac{NE\Delta L_1}{L_1 - L_{s1}}\right)^2 + \left(\frac{NE\Delta L_2}{L_2 - L_{s2}}\right)^2 \right]^{1/2}. \tag{18}$$

The depth error is in general minimized by choosing wavelength bands with the smallest attenuation. In the ratio method, however, the sensitivity to noise increases rapidly as the difference between the attenuation coefficients in the two bands decreases. Since this difference is only 0.025 m^{-1} in the above example, these are not the optimum wavelengths for the ratio method. For any choice of wavelengths, however, the depth error due to noise is larger for the ratio method than for the method described above. The ratio method is also subject to errors due to changes in bottom composition: although these can be reduced by an appropriate choice of wavelengths, they can never in practice be completely eliminated.

Conclusions

The ratio algorithms for water depth and bottom features mapping are relatively simple techniques which give acceptable results in many situations. However, these algorithms are limited by operational restrictions which reduce their applicability and utility. A more general algorithm has been defined, and a preliminary evaluation of this method has been performed using a simulation model for the water radiance.

The advantages of this method for mapping bottom features are (1) increased operational flexibility, in that the wavelength bands are not limited to those with equal water attenuation coefficients, (2) better discrimination of bottom materials with similarly shaped reflectance spectra, and (3) improved performance through the use of more than two wavelengths bands.

The advantages of this method for mapping water depth are (1) increased operational flexibility, since the wavelength bands are not restricted by the requirement of equal bottom reflectance ratios for all bottom types, (2) lower sensitivity to noise, and (3) improved performance through the use of more than two wavelength bands.

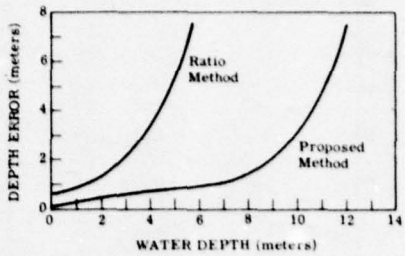

Fig. 4. Total depth error using the proposed method and depth error due to noise using the ratio method for water and bottom types shown in Fig. 1.

The disadvantage of the algorithm defined here is that it is more complex and therefore somewhat more difficult to implement than the ratio methods. The subtraction and division operations required for the ratio methods can be implemented by either analog or digital processors, whereas the method defined here requires digital computation. The input parameters for this algorithm are also somewhat more difficult to determine than those for the ratio methods.

Numerical results illustrating the performance of this method have been presented for one example situation. These results should not be considered as definitive of the best possible performance, since the wavelengths considered are not necessarily the optimum ones nor are the reflectances used necessarily representative of actual bottom types. In addition, better performance can be obtained by reducing system noise and by using more than two wavelength bands. The value of $NE\Delta L$ used in these calculations was 0.05 mW cm^{-2} sr^{-1} μm^{-1}. This is a typical value for an aircraft multispectral scanner with an angular field of view of a few milliradians, a spectral resolution of about 0.025 μm, and a collector area of about 80 cm^2. This noise equivalent radiance can readily be reduced by a factor of 2 or 3, with a corresponding reduction in the depth error, by increasing the collector area or reducing the spatial or spectral resolution of the system.

This work was supported by the Office of Naval Research, contract N000-14-74-C-0273.

Appendix A: Shallow-Water Radiance Model

The radiances shown in Fig. 1 were calculated using a combined water–atmosphere radiance model which includes the effects of scattering in the atmosphere and reflection at the water surface, as well as the components originating in the water itself. The atmospheric effects are calculated from the double-delta approximation,[9] using the atmospheric parameters tabulated by Elterman.[10] A solar zenith angle of 20° and a platform altitude of 1 km were used for the calculations in this report.

The water radiance is calculated using the quasi-single-scattering approximation,[11] modified to include the effects of reflection from the bottom[12] and internal reflection at the water surface.[13] The effects of internal reflection are included to all orders by assuming that the upwelling radiance distribution just beneath the water surface has a uniform angular distribution. Thus, the upwelling underwater radiance can be written as $L(\mu',\phi)$

$$= \frac{E_0' S(\mu',\mu_0',\phi) + \int_0^1 \int_0^{2\pi} L'(\mu'',\phi'') S(\mu',\mu'',\phi'') \mu'' d\mu'' d\phi''}{1 - \int_0^1 \int_0^{2\pi} R(\mu'') S(\mu',\mu'',\phi'') \mu'' d\mu'' d\phi''}, \quad \text{(A1)}$$

where E_0' is the direct solar irradiance penetrating the water surface, $L'(\mu'',\phi'')$ is the transmitted sky radiance below the surface, μ_0' is the cosine of the apparent solar zenith angle below the surface, $R(\mu'')$ is the Fresnel reflectance of the water surface, and

$$S(\mu,\mu',\phi) = \frac{1}{K}(\mu + \mu')^{-1} \left\{1 - \exp\left[-\left(\frac{1}{\mu} + \frac{1}{\mu'}\right) Kz\right]\right\} \beta(\mu_s) + \frac{r_B}{\pi} \exp\left[-\left(\frac{1}{\mu} + \frac{1}{\mu'}\right) Kz\right], \quad \text{(A2)}$$

where K is the irradiance attenuation coefficient,[14] z is the water depth, $\beta(\mu_s)$ is the volume scattering function, r_B is the bottom reflectance, and

$$\mu_s = -\mu\mu' + [(1-\mu^2)(1-\mu'^2)]^{1/2} \cos\phi. \quad \text{(A3)}$$

The results of this model agree with exact calculations using the Monte Carlo method[15] to within about 10% for values of the single-scattering albedo less than 0.8 and bottom reflectances less than 50%.

Appendix B: Coordinate System Rotation Parameters

The assumption involved in making the coordinate transformation (8) is that the variables X_i are linearly correlated with the water depth z, that is,

$$\hat{X}_i = a_i - b_i z \quad \text{(B1)}$$

with possibly different values of a_i for each bottom type. It is desired to transform this set of N depth-dependent variables into a new set of $N-1$ depth-independent variables ($Y_1 \ldots Y_{N-1}$) and one depth-dependent variable (Y_N). The required transformation may be visualized as a pure rotation in N-space such that the Y_N axis is oriented in the direction specified by the parametric Eq. (B1). Thus, the transformation parameters for Y_N are

$$A_{Nj} = b_j \left(\sum_{k=1}^{N} b_k^2\right)^{-1/2}. \quad \text{(B2)}$$

The remaining parameters can be calculated using the conditions for the orthonormality of the new coordinate axes

$$\sum_{k=1}^{N} A_{ik} A_{jk} = \begin{cases} 0, i \neq j \\ 1, i = j \end{cases} \quad \text{(B3)}$$

and the condition for a proper rotation

$$\det(A_{ij}) = 1. \quad \text{(B4)}$$

These conditions uniquely define the transformation matrix only for the case $N = 2$. For three or more dimensions, however, a unique solution can be obtained by requiring that the coefficients for $Y_1 \ldots Y_{N-1}$ be the same for the $(N+1)$-dimensional case as for the N-dimensional case. The coefficients for the $(N-1)$ depth-independent variables are then

$$A_{ij} = b_{i+1} b_j \left(\sum_{k=1}^{i} b_k^2\right)^{-1/2} \left(\sum_{k=1}^{i+1} b_k^2\right)^{-1/2} \quad \text{for } j = 1 \ldots i, \quad \text{(B5)}$$

$$A_{ij} = -\left(\sum_{k=1}^{i} b_k^2\right)^{1/2} \left(\sum_{k=1}^{i+1} b_k^2\right)^{-1/2} \quad \text{for } j = i+1, \quad \text{(B6)}$$

$$A_{ij} = 0 \quad \text{for } j = i+2 \ldots N. \quad \text{(B7)}$$

These equations, along with Eq. (B2), completely define the required coordinate transformation. The values of b_i can be calculated if the water attenuation coefficients are known or can be empirically obtained from a regression analysis of the measured radiance values over a uniform bottom.

References

1. F. C. Polcyn, W. L. Brown, and I. J. Sattinger, "The Measurement of Water Depth by Remote Sensing Techniques," Report 8973-26-F, Willow Run Laboratories, The University of Michigan, Ann Arbor (1970).
2. C. T. Wezernak and D. R. Lyzenga, Remote Sensing Environ. **4,** 37 (1975).
3. F. C. Polcyn and D. R. Lyzenga, "Calculation of Water Depth from ERTS—MSS Data," in *Proceedings Symposium on Significant Results Obtained from ERTS-1,* NASA Publication SP-327 (1973).
4. D. Lyzenga and F. Thomson, "Data Processing and Evaluation for Panama City Coastal Survey: Bathymetry Results," Report 121400-1-T, Environmental Research Institute of Michigan, Ann Arbor, Mich. (1976).
5. N. G. Jerlov, *Optical Oceanography* (Elsevier, New York, 1968).
6. T. J. Petzold, "Volume Scattering Functions for Selected Ocean Waters," Visibility Laboratory Tech. Report 72-78, Scripps Institution of Oceanography, San Diego, Calif. (1972).
7. J. L. Mueller, Appl. Opt. **15,** 394 (1976).
8. W. R. McCluney, Remote Sensing Environ. **5,** 3 (1976).
9. W. A. Malila, R. B. Crane, C. A. Omarzu, and R. E. Turner, Studies of Spectral Discrimination, Report 31650-22-T, Willow Run Laboratories, University of Michigan, Ann Arbor (1971).
10. L. Elterman, "UV, Visible and IR Attenuation for Altitudes to 50 km," Report AFCRL-68-0153, Air Force Cambridge Research Laboratories, Bedford, Mass. (1970).
11. H. R. Gordon, Appl. Opt. **12,** 2803 (1973).
12. W. R. McCluney, "Estimation of Sunlight Penetration in the Sea for Remote Sensing," NASA Report TM X-70643 (1974).
13. D. R. Lyzenga, Appl. Opt. **16,** 282 (1977).
14. The use of K instead of $c^* = (1 - w_0 F)c$ in the quasi-single-scattering approximation represents a further approximation, which is valid if K is measured under direct solar illumination with the sun near zenith, see H. R. Gordon, J. Opt. Soc. Am. **64,** 773 (1974).
15. H. R. Gordon and O. B. Brown, Appl. Opt. **13,** 2153 (1974).

REFERENCES

1. F. Thomson, R. Shuchman, C. Wezernak, D. Lyzenga, and D. Leu, Basic Remote Sensing Investigation for Beach Reconnaissance, ERIM Report No. 108900-5-P, 1976.

2. D. Lyzenga, R. Shuchman, F. Thomson, C.F. Davis, and G.H. Suits, Basic Remote Sensing Investigation for Beach Reconnaissance, ERIM Report No. 108900-9-P, 1977.

3. D.R. Lyzenga, Passive Remote Sensing Techniques for Mapping Water Depth and Bottom Features, Applied Optics, 17, 379, 1978.

4. D.R. Lyzenga and F.J. Thomson, Detectability of Black Submerged Objects, ERIM Report No. 123500-1-F, 1976.

5. D.R. Lyzenga, C.T. Wezernak, and F.C. Polcyn, Spectral Band Positioning for Purposes of Bathymetry and Mapping Bottom Feature from Satellite Altitudes, ERIM Report No. 115300-5-T, 1976.

6. D.R. Lyzenga and F.C. Polcyn, Tidal Affected Distributions of Surface Chlorophyll and Transparency in tne New York Bight, ERIM Report No. 122600-1-F, 1977.

7. D.R. Lyzenga and F.C. Polcyn, Analysis of Optimum Spectral Resolution and Band Location for Satellite Bathymetry, ERIM Report No. 128200-1-F, 1978.

8. H.R. Gordon, Simple Calculation of the Diffuse Reflectance of the Ocean, Applied Optics, 12, 2803, 1973.

9. R.E. Turner, Radiative Transfer in Real Atmospheres, ERIM Report No. 190100-24-T, 1974.

10. Steve Stewart, Mission Report for Naval Coastal Systems Laboratory Program, ERIM Report No. 128500-2-L, 1977.

11. Robert A. Arnone, Water Properties for the Gulf and Bay Waters in Support of ERIM Project, 25-26 May 1977, NCSL Report No. SP 77-G-56, 1977.

12. T.J. Petzold, Volume Scattering Functions for Selected Ocean Waters, Visibility Laboratory Tech. Report No. 72-78, Scripps Institute of Oceanography, San Diego, CA, 1972.

13. N.G. Jerlov, Optical Oceanography (Elsevior, New York, 1968).

14. R.A. Shuchman and D.R. Lyzenga, Active-Passive Scanner Bathymetry and Land Feature Classification Results-Panama City, Florida, 1977, ERIM Report No. 128500-4-T, 1977.

DISTRIBUTION LIST

Office of Naval Research
Geography Programs
Code 462
Arlington, Virginia 22217
2 copies

Defense Documentation Center
Cameron Station
Alexandria, Virginia 22314
12 copies

Director, Naval Research Lab
Attention: Technical Information Officer
Washington, D.C. 20375
6 copies

Director,
Office of Naval Research Branch Office
1030 East Green Street
Pasadena, California 91101

Director,
Office of Naval Research Branch Office
536 South Clark Street
Chicago, Illinois 60605

Director,
Office of Naval Research Branch Office
495 Summer Street
Boston, Massachusetts 02210

Commanding Officer
Office of Naval Research Branch Office
Box 39
FPO New York 09510

Chief of Naval Research
Asst. for Marine Corps Matters
Code 100M
Office of Naval Research
Arlington, Virginia 22217

NORDA
Code 400
National Space Technology Laboratories
Bay St. Louis, Mississippi 39520

Office of Naval Research
Operational Applications Division
Code 200
Arlington, Virginia 22217

Office of Naval Research
Scientific Liaison Officer
Scripps Institution of Oceanography
La Jolla, California 92093

Director, Naval Research Laboratory
Attention: Library, Code 2628
Washington, D.C. 20375

ONR Scientific Liaison Group
American Embassy - Room A-407
APO San Francisco 96503

Commander
Naval Oceanographic Office
Attention: Library Code 1600
Washington, D.C. 20374

Naval Oceanographic Office
Code 3001
Washington, D.C. 20374

Chief of Naval Operations
OP 987P1
Department of the Navy
Washington, D.C. 20350

Oceanographer of the Navy
Hoffman II Building
200 Stovall Street
Alexandria, Virginia 22322

Naval Academy Library
U.S. Naval Academy
Annapolis, Maryland 21402

Commanding Officer
Naval Coastal Systems Laboratory
Panama City, Florida 32401

Librarian
Naval Intelligence
Support Center
4301 Suitland Road
Washington, D.C. 20390

Officer in Charge
Environmental Research Prdctn. Fclty.
Naval Postgraduate School
Monterey, California 93940

Commanding General
Marine Corps Development and Educational Command
Quantico, Virginia 22134

Dr. A. L. Slafkosky
Scientific Advisor
Commandant of the Marine Corps
Code MC-RD-1
Washington, D.C. 20380

Defense Intelligence Agency
Central Reference Division
Code RDS-3
Washington, D.C. 20301

Director
Defense Mapping Topographic Center
Attention: Code 50200
Washington, D.C. 20315

Commanding Officer
U.S. Army Engineering
Topographic Laboratory
Attention: ETL-ST
Fort Belvoir, Virginia 22060

Chief, Wave Dynamics Division
USAE-WES
P.O. Box 631
Vicksburg, Mississippi 39180

National Oceanographic Data
Center D764
Environmental Data Services
NOAA
Washington, D.C. 20235

Central Intelligence Agency
Attention: OCR/DD-Publications
Washington, D.C. 20505

Dr. Mark M. Macomber
Advanced Technology Division
Defense Mapping Agency
Naval Observatory
Washington, D.C. 20390

Ministerial Direktor Dr. F. Wever
RUE/FO
Bundesministerium der Verteidigung
Hardthoehe
D-5300 Bonn, West Germany

Oberregierungstrat Dr. Ullrich
Rue/FO
Bundesministerium der Verteidigung
Hardthoehe
D-5300 Bonn, West Germany

Mr. Tage Strarup
Defence Research Establishment
Osterbrogades Kaserne
DK-2100 Koberhavn O, Denmark

IR. M. W. Van Batenberg
Physisch Laboratorium INO
Oude Wallsdorper Weg 63, Den Haag
Netherlands

Dr. Gordon E. Carlson
University of Missouri
Department of Electrical Engineering
Rolla, Missouri 65401

Coastal Studies Institute
Louisiana State University
Baton Rouge, Louisiana 70803

Dr. Bernard Le Mehaute
Tetra Tech. Inc.
630 North Rosemead Boulevard
Pasadena, California 91107

Dr. William S. Gaither
Dean, College of Marine Studies
Robinson Hall
University of Delaware
Newark, Delaware 19711

Dr. Lester A. Gerhardt
Rennsselaer Polytechnic Institute
Troy, New York 12181

Mr. Fred Thomson
Environmental Research Institute of Michigan
P. O. Box 8618
Ann Arbor, Michigan 48107

Dr. J. A. Dracup
Environmental Dynamics, Inc.
1609 Westwood Boulevard, Suite 202
Los Angeles, California 90024

Dr. Thomas K. Peucker
Simon Fraser University
Department of Geography
Burnaby 2, B.C., Canada

Dr. Bruce Hayden
Department of Environmental Sciences
University of Virginia
Charlottesville, Virginia 22903